Computational Fluid Dynamics Modeling of Nickel Hydrogen Batteries

R. Cullion, W.B. Gu, C.Y. Wang
GATE Center for Advanced Energy Storage
Department of Mechanical and Nuclear Engineering
Pennsylvania State University
University Park, PA 16802

P. Timmerman
Jet Propulsion Laboratory
Pasadena, CA 91109

Abstract

An electrochemical Ni-H_2 battery model has been expanded to include thermal effects. A thermal energy conservation equation was derived from first principles. An electrochemical and thermal coupled model was created by the addition of this equation to an existing multiphase, electrochemical model. Charging at various rates was investigated and the results validated against experimental data. Reaction currents, pressure changes, temperature profiles, and concentration variations within the cell are predicted numerically and compared with available data and theory.

Introduction

The nickel hydrogen battery provides an important form of energy storage. This battery has applications in both the aerospace and the electric vehicle industries. Nickel hydrogen batteries are used in these fields due to their ability to provide long cycle lifetimes, high specific energy, high power density, and high tolerance to overcharge.

Demands by industry have made mathematical modeling of these batteries crucial, in particular, thermal modeling has become essential. Temperature variations within the battery influence the performance, life, and reliability of the power source. At low temperatures there are capacity losses due to high internal resistance within the battery and at high temperatures the capacity is compromised by fast self-discharge. Use of the active material must be balanced in order to maximize battery life. To do this a uniform temperature profile is necessary. Modeling provides a way to monitor the temperature profiles, and a way to test improvements without running lengthy and expensive experiments. Another very important reason thermal modeling is essential is safety. Side reactions occurring within the battery often result in temperature increases, which could lead to thermal runaway. Modeling would allow the runaway to be predicted.

The cell electrochemical behavior is described by electrochemical reactions that are affected by temperature-dependent electrochemical and transport properties. This interrelation of the electrochemical reactions and temperature-dependent properties makes it necessary to couple the electrochemical and thermal models of the Ni-H_2 cell into a single comprehensive model. Incorporating the thermal energy conservation

equation, in which the local heat generation rate is determined by the electrochemical processes, into the model achieves the coupling.

A one-dimensional, thermal and electrochemical model has been developed by DeVidt et. Al [2]. The transport phenomena of the gaseous species and electrolyte within the cell were described using concentrated solution theory and the volume averaging technique. A pseudo-second dimension was used to model the proton diffusion inside the active material. Three reactions in the nickel electrode were considered. The main reaction was the oxidation/reduction of the nickel species into the solid active material, and the side reactions were oxygen evolution/reduction and oxidation of dissolved hydrogen. The present work provides a two-dimensional, fully coupled, thermal and electrochemical model. It also makes use of the volume averaging technique and concentrated solution theory [8]. Unlike the model developed by DeVidt et. al. [2], the present work employs a multiphase reaction scheme. At the nickel electrode two main reactions are considered. Oxidation/reduction reactions of the nickel species in both the beta and gamma phases are considered. The side reactions, oxygen evolution/reduction and oxidation of dissolved hydrogen, are also included. The gamma phase is less stable than the beta phase and occurs mainly during overcharge [6]. Adding both the beta and gamma phase reactions to the model allows for more accurate prediction of the discharge/charge behavior as was demonstrated by Timmerman [7].

DeVidt's work [2] considers the cell to be isothermal spatially. An adiabatic case and an isothermal case were investigated. The focus of this study is to create an axisymmetric, multidimensional, thermal and electrochemical coupled model. The multidimensional nature of the present model is necessary because temperature gradients in the Ni-H_2 cell are present mainly in the radial direction due to heat dissipation through the battery wall, while the electrochemical and ion transport processes occur in the axial direction. Temperature gradients within the cell will be determined by this model due to their importance in predicting cell performance, making improvements, and for safety purposes. The energy equation of the two-dimensional model will include a heat generation term that incorporates the heat effects due to electrochemical reactions, joule heating, and phase changes of non-electrochemical nature. Also, as mentioned earlier, DeVidt's model [2] considered two extreme boundary conditions, an adiabatic case and an isothermal case. This model allows for a general convective boundary condition.

Thermal-Electrochemical Model

A single Ni-H_2 cell consists of an aluminum current collector, a nickel electrode, a separator, a hydrogen electrode (which has a micro-porous Teflon membrane backing permeable only to gas), a nickel current collector, and a gas diffusion screen, as shown schematically in Fig. 1. A concentrated KOH aqueous solution serves as the electrolyte. The Ni-H_2 battery is composed of a stack of these disk-shaped cells housed within a pressure vessel [3]. The cells are center aligned within the vessel. There is an outer gap between the wall of the pressure vessel and the circumference of the cell stack to ensure electric insulation between the cell stack and the pressure vessel and to provide a path for hydrogen gas to diffuse from the external reservoir into the cell stack. It is important to note the cell is axisymmetric, therefore although only the radial and axial directions will be examined the results will be the same as those found for a three-dimensional case.

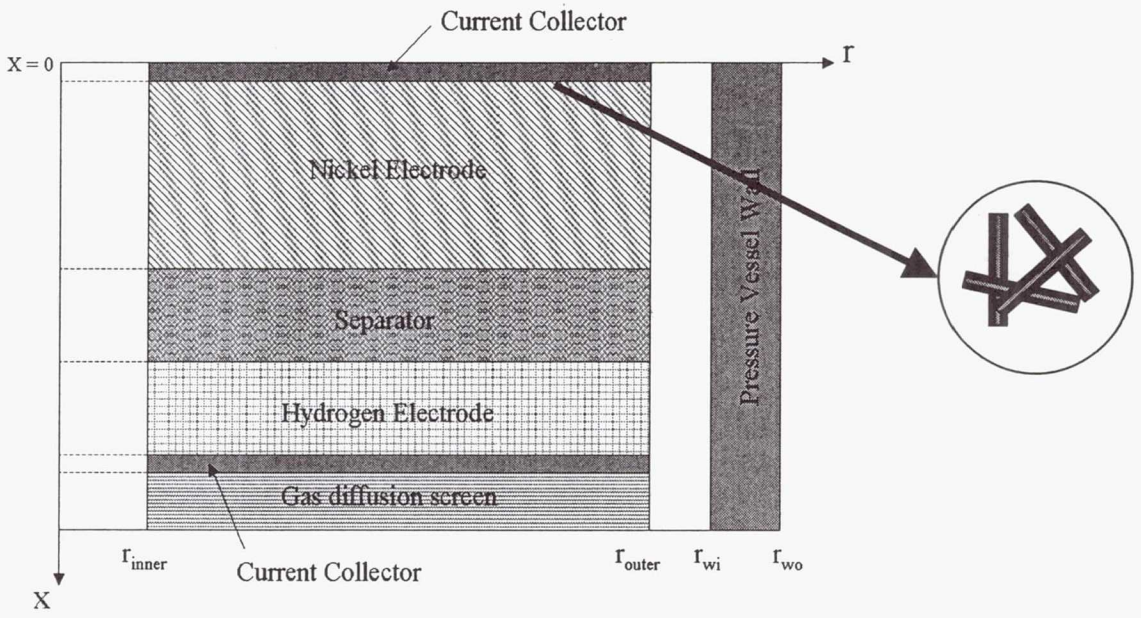

Figure 1. Schematic Representation of a Ni-H_2 Cell

Assumptions

The present work is based on the following assumptions. This problem is considered to be axisymmetric. The convection effect between the outer edge of the cell and the pressure vessel wall, important when the temperature difference between the two is large, is ignored for simplicity. As a result, in this space the species transport is by diffusion and migration only and the heat transfer is by conduction only. The nickel electrode consists of composite cylindrical needles with a substrate inside (see Fig. 1). The active material film is assumed to be a mixture of multiple phases with a constant diffusion coefficient for the protons. Furthermore, the α and γ phases are treated as a single phase [7]. The electrode porosities are considered to be constant. There is a continuous gas-pore network throughout the cell with a uniform constant volume fraction. The gas, a mixture of hydrogen, oxygen, and water vapor, is ideal. Its composition varies with time but does not change with position [1]. The solid phase is assumed to be completely wetted by the electrolyte film. Interfacial chemical equilibrium exists in the liquid phase for all species other than the dissolved oxygen that has a small value of mass diffusivity in the liquid electrolyte. Electrical equilibrium exists in the liquid phase due to the large value of ionic conductivity of the electrolyte. Finally it can be said that the combined thickness of the current collector and the Ni electrode is much smaller than the diameter of the cell, therefore ϕ_{sub} is considered to be constant along x but to vary with r.

Model Equations

At the nickel electrode the following main reactions occur:

β phase reaction:

$$NiOOH_{\beta} + H_2O + e^- \Leftrightarrow Ni(OH)_{2,\beta} + OH^- \quad (1a)$$

γ phase reaction:

$$NiOOH_{\gamma} + H_2O + ne^- \Leftrightarrow Ni(OH)_{2,\alpha} + OH^- \quad (1b)$$

γ phase production:

$$NiOOH_{\beta} + ne^- + K^+ \rightarrow NiOOH_{\gamma} + OH^- \quad (1c)$$

α phase reconversion:

$$Ni(OH)_{2,\alpha} \rightarrow Ni(OH)_{2,\beta} \quad (1d)$$

Oxygen evolution/reduction and the oxidation of dissolved hydrogen also occur at the nickel electrode and are considered to be side reactions:

$$\frac{1}{2}O_2 + H_2O + 2e^- \Leftrightarrow 2OH^- \quad (2)$$

$$2H_2O + 2e^- \leftarrow H_2 + 2OH^- \quad (3)$$

Two reactions occur at the hydrogen electrode, the main reaction:

$$H_2 + 2OH^- \Leftrightarrow 2H_2O + 2e^- \quad (4)$$

and the side reaction is:

$$2OH^- \leftarrow \frac{1}{2}O_2 + H_2O + 2e^- \quad (5)$$

The general Butler-Volmer equation is used to determine the rates at which these reactions occur. The equations are written with respect to a specified reference state, namely a temperature of 10°C and an electrolyte concentration of 7.1d-3 mol/cm^3.

$$\bar{i}_{n1a} = i_{o1a,ref}\left[\left(\frac{c^{OH}}{c^{OH}_{ref}}\right)\left(\frac{c_{\beta}^{-H}}{c^{H}_{\beta ref}}\right)\exp\left(\frac{\alpha_{a1a}F}{RT}\eta_{1a}\right) - \left(\frac{c^{H}_{\beta\max} - c_{\beta}^{-H}}{c^{H}_{\beta\max} - c^{H}_{\beta ref}}\right)\exp\left(-\frac{\alpha_{c1a}F}{RT}\eta_{1a}\right)\right] \quad (6)$$

$$\bar{i}_{n1b} = i_{o1b,ref}\left[\left(\frac{c^{OH}}{c^{OH}_{ref}}\right)\left(\frac{c_{\gamma}^{-H}}{c^{H}_{\gamma ref}}\right)\exp\left(\frac{\alpha_{a1b}F}{RT}\eta_{1b}\right) - \left(\frac{c^{H}_{\gamma\max} - c_{\gamma}^{-H}}{c^{H}_{\gamma\max} - c^{H}_{\gamma ref}}\right)\exp\left(-\frac{\alpha_{c1b}F}{RT}\eta_{1b}\right)\right] \quad (7)$$

$$\bar{i}_{n1c} = 2i_{o1c,ref}\left[1 - \left(\frac{c_{\beta}^{-H}}{c^{H}_{\beta\max}}\right)\exp\left(-\frac{\alpha_{c1c}F}{RT}\eta_{1c}\right)\right] \quad (8)$$

$$\bar{i}_{n2} = i_{o2,ref}\left[\left(\frac{c^{OH}}{c^{OH}_{ref}}\right)^2 \exp\left(\frac{\alpha_{a2}F}{RT}\eta_2\right) - \left(\frac{c_e^{-O_2}}{c^{O_2}_{eref}}\right)\exp\left(-\frac{\alpha_{c2}F}{RT}\eta_2\right)\right] \tag{9}$$

$$\bar{i}_{n3} = i_{o3,ref}\left[\left(\frac{c^{OH}}{c^{OH}_{ref}}\right)^2\left(\frac{c_e^{-H_2}}{c^{H_2}_{eref}}\right)\exp\left(\frac{\alpha_{a3}F}{RT}\eta_3\right) - \exp\left(-\frac{\alpha_{c3}F}{RT}\eta_3\right)\right] \tag{10}$$

$$\bar{i}_{n4} = i_{o4,ref}\left[\left(\frac{c^{OH}}{c^{OH}_{ref}}\right)^2\left(\frac{c_e^{-H_2}}{c^{H_2}_{eref}}\right)\exp\left(\frac{\alpha_{a4}F}{RT}\eta_4\right) - \exp\left(-\frac{\alpha_{c4}F}{RT}\eta_4\right)\right] \tag{11}$$

$$\bar{i}_{n5} = i_{o5,ref}\left[\left(\frac{c^{OH}}{c^{OH}_{ref}}\right)^2 \exp\left(\frac{\alpha_{a5}F}{RT}\eta_5\right) - \left(\frac{c_e^{O_2}}{c^{O_2}_{eref}}\right)\exp\left(-\frac{\alpha_{c5}F}{RT}\eta_5\right)\right] \tag{12}$$

The subscripts in the above equations; 1a, 1b, 1c, 2, 3, 4, 5 refer to the reactions labeled with the respective equation number.

The overpotential of a given reaction j, η_j, is given by [4]:

$$\eta_j = \phi_{se} - \phi_e - \left(U_{j,ref} + \left(T - T_{ref}\right)\left(\frac{\partial U}{\partial T} - \frac{\partial U_{ref}}{\partial T}\right)\right) \tag{13}$$

The temperature dependency of the overpotential is considered in the above equation. The reference overpotentials for the nickel electrode are calculated using the following equations [7]:

$$U_{1*,ref} = U^o_{1*} - \frac{RT}{F}\ln\left(\frac{c^H_{sref}}{c^H_{s\max} - c^H_{sref}}\right) + \frac{RT}{F}k\left(2\theta_s - 1\right) \tag{14}$$

$$U_{1c,ref} = U^o_{1c} \tag{15}$$

and the reference overpotentials for the oxygen and hydrogen reactions are [1]:

$$U_{3,ref} = U_{4,ref} = -0.9263 - \frac{RT}{2F}\ln\left(p^{H_2}_{ref}\right) \tag{16}$$

$$U_{2,ref} = U_{5,ref} = 0.3027 + \frac{RT}{4F}\ln\left(p^{O_2}_{ref}\right) \tag{17}$$

k in equation 14 is an intercalation constant used to describe the interaction between species in a solid solution.

The conservation of OH species in the liquid phase is represented by the following equation [7]:

$$\frac{\partial\left(\varepsilon_e c^{OH}\right)}{\partial t} = \nabla\left(D^{OH}_{eff}\nabla c^{OH}\right) + \frac{t^o_- - 1}{F}j^{OH} \tag{18}$$

where t^o_- is the transference number of OH^- with respect to the velocity of the solvent. j^{OH} is the total transfer current from all electrochemical reactions that generate or consume OH at the electrode/electrolyte interface:

$$j^{OH} = \begin{cases} j_b^{OH} + j_g^{OH} & \text{in the nickel electrode} \\ 0 & \text{in the separator} \\ a_H(\bar{i}_{n4} + \bar{i}_{n5}) & \text{in the hydrogen electrode} \end{cases} \quad (19)$$

where

$$j^{OH}_{\beta} = a_{Ni}(1 - X_{\gamma})[\bar{i}_{n1a} + (\bar{i}_{n2} + \bar{i}_{n3})_{\beta}] \quad (20)$$

$$j_{\gamma}^{OH} = a_{Ni}X_{\gamma}[\bar{i}_{n1b} + (\bar{i}_{n2} + \bar{i}_{n3})_{\gamma}]$$

Similarly, j^{H}_2 and j^{O}_2 are the transfer currents associated with the generation or consumption of hydrogen and oxygen respectively:

$$j^{H2} = \begin{cases} a_{Ni}\bar{i}_{n3} & \text{in the nickel electrode} \\ 0 & \text{in the separator} \\ a_H\bar{i}_{n4} & \text{in the hydrogen electrode} \end{cases} \quad (21)$$

$$j^{O2} = \begin{cases} a_{Ni}\bar{i}_{n2} & \text{in the nickel electrode} \\ 0 & \text{in the separator} \\ a_H\bar{i}_{n5} & \text{in the hydrogen electrode} \end{cases} \quad (22)$$

Conservation of H_2 species in the liquid phase is given by [7]:

$$\frac{\partial\left(\varepsilon_e C_e^{H_2}\right)}{\partial t} = \nabla\left(D_{eff}^{H_2}\nabla c_e^{H_2}\right) + \frac{1}{2F} j^{H_2} + J_{eg}^{H_2} \quad (23)$$

O_2 species conservation in the liquid phase is [7]:

$$\frac{\partial\left(\varepsilon_e c_e^{O_2}\right)}{\partial t} = \nabla\left(D_{eff}^{O_2}\nabla c_e^{O_2}\right) + \frac{1}{4F} j^{O_2} + J_{eg}^{O_2} \quad (24)$$

The interfacial mass transfer rate of the hydrogen or oxygen from the liquid to the gas phase is expressed as:

$$J^{i}_{eg} = K^{i}\left(\frac{H^{i}}{RT}c^{i}_{g} - c^{i}_{e}\right) \qquad i = H_2 \text{ and } O_2 \tag{25}$$

Conservation of species in the gas phase is given as [7]:

$$\frac{\partial\left(c_g^i\right)}{\partial t} = \frac{-1}{V_g}\int_v J^i_{eg}\,dV \tag{26}$$

Conservation of species in the solid phase [7]:

$$\frac{\partial\left(\varepsilon_e c_s^H\right)}{\partial t} = \frac{j_s^H}{F} \tag{27}$$

where

$$j^{H}_{s} = \begin{cases} a_{Ni}(1 - X_g)\bar{i}_{n1a} & \text{for } s = b \\ a_{Ni}X_g\bar{i}_{n1b} & \text{for } s = g \end{cases} \tag{28}$$

Conservation of charge in the liquid phase is represented by [7]:

$$\nabla\cdot\left(k^{eff}\nabla\phi_e\right) + \nabla\left(k_d^{eff}\nabla\ln c^{OH}\right) + j^{OH} = 0 \tag{29}$$

Conservation of charge in the solid phase is given [7]:

$$\nabla\left(\sigma_s^{eff}\nabla\phi_s\right) - j_s^{OH} + a_{sb}\frac{\bar{\phi}_{sb} - \phi_s}{R_{sb}} = 0 \tag{30}$$

The energy conservation equation is written in the following form [4]:

$$\rho C_p\frac{\partial T}{\partial t} = \nabla\lambda\nabla T + q''' \tag{31}$$

where

$$\rho C_p = \varepsilon_e\rho_e C_p + \varepsilon_s\rho_s C_p + \varepsilon_g\rho_g C_p \tag{31a}$$

$$\lambda = \varepsilon_e\lambda_e^{eff} + \varepsilon_s\lambda_s^{eff} + \varepsilon_g\lambda_g^{eff} \tag{31b}$$

The third term of the energy equation has three components. The first part:

$$\frac{1}{V}\int_V a_{se}\sum \bar{i}_{nj}\left(\overline{\eta}_j + \Pi_j\right)dV \tag{32}$$

represents the heat effect produced by the electrochemical reactions [4]. This component includes both the reversible heat characterized by the Peltier coefficient:

$$\Pi_j = T\frac{\partial U_j}{\partial t} \tag{33}$$

and the irreversible heat related to the surface overpotential.

The second component of the heat generation term is associated with phase changes of the non-electrochemical nature, e.g. evaporation or condensation of water within the cell [4]:

$$\sum \Delta h \cdot \Gamma = \Delta h_{\alpha\beta} r_{\alpha\beta} + \Delta h_{eg}^{H_2O} J_{eg}^{H_2O} \tag{34}$$

The third component of the heat generation term:

$$\frac{1}{V}\int_V \sum_\sigma \left(\sigma_s^{eff}\nabla\phi_s + k^{eff}\nabla\phi_e\nabla\phi_e + k_D^{eff}\nabla \ln c^{OH}\cdot\nabla\phi_e\right)dV \tag{35}$$

represents the joule heating in both the solid and liquid phases [4].

Electrochemical and transport properties that are temperature dependent are expected to follow the Arrhenius equation [4]:

$$\Phi = \Phi_o \exp\left(-\frac{E_{act}}{R}\left(\frac{1}{T}-\frac{1}{T_o}\right)\right) \tag{36}$$

where E_{act} is the activation energy corresponding to a property Φ.

The top and bottom of the cell were considered to be adiabatic. The thermal boundary condition applied to the inner edge of the cell and the outer wall of the pressure vessel was the following:

$$-k\frac{\partial T}{\partial r} = h(T - T_{environment}) \tag{37}$$

where k is the thermal conductivity of the material, and h is the heat transfer coefficient.

Results and Discussion

Cell performance under various conditions was simulated using the model described above. Physical properties and electrochemical parameters were provided from experimental work conducted at JPL and are listed in Table I. Several parameters were

not available, but found through trial and error to produce the best overall agreement with experimental charge data (these values are indicated with an asterisk).

Table 1: Parameters

Parameter	Values	References
Kinetics		
$i_{o,1a}$	3.0d-04 A/cm^2	*
$i_{o,1b}$	1.0d-04 A/cm^2	
$i_{o,1c}$	2.0d-55 A/cm^2	
$i_{o,2}$	3.0d-10 A/cm^2	*
$i_{o,3}$	2.5d-16 A/cm^2	*
$i_{o,4}$	6.5d-05 A/cm^2	*
$i_{o,5}$	1.0d-07 A/cm^2	*
α_{1a}	5.0d-01 A/cm^2	
α_{1b}	5.0d-01 A/cm^2	
α_{1c}	5.0d-01 A/cm^2	
α_2	1.0d+00 A/cm^2	
α_3	5.0d-01 A/cm^2	
α_4	5.0d-01 A/cm^2	
α_5	1.0d+00 A/cm^2	
$P_{hydrogen,ref}$	52.0 Atm	Ref 1
$P_{oxygen,ref}$	5.0e-4 Atm	Ref 1
U_{1a}	4.2d-01 V	
U_{1b}	3.35d-1 V	
U_{1c}	4.4d-01 V	
U_2	3.0d-01 V	
U_3	-9.26d-1 V	
U_4	-9.26d-1 V	
U_5	3.0d-01 V	
E_{1a}	5.0d+04 J/mol	
E_{1b}	3.0d+04 J/mol	
E_{1c}	0.0d+00 J/mol	
E_2	8.0d+04 J/mol	
E_3	0.0d+00 J/mol	
E_4	2.0d+04 J/mol	
E_5	1.2d+05 J/mol	
Thermal		
$dudt_{1a}$	-2.11d-3 V/K	
$dudt_{1b}$	-1.51d-3 V/K	
$dudt_{1c}$	0.0d+00 V/K	
$dudt_2$	-1.68d-3 V/K	
$dudt_3$	-8.36d-3 V/K	
$dudt_4$	-8.36d-3 V/K	
$dudt_5$	-1.68d-3 V/K	
initial temperature	15°C	
reference temperature	15°C	
environmental temperature	0°C	

heat transfer coefficient	5 W/m^2K	*
Cell		
electrode pairs	17	
inner pressure vessel radius	4.435 cm	
outer electrode radius	4.400 cm	
inner electrode radius	0.350 cm	
Al current collector thickness	0.0015 cm	
Ni electrode thickness	0.453 cm	
Separator thickness	0.210 cm	
Pt H_2 electrode thickness	0.400 cm	
Ni current collector thickness	0.0010 cm	
Gas screen thickness	0.0610 cm	
Porosity of substrate	0.85	
Porosity of Ni electrode	0.41	
Porosity of Pt H_2 electrode	0.85	
Porosity of separator	0.85	
Specific interfacial area of substrate	2000 cm^2/cm^3	
Specific interfacial area of nickel electrode	3919 cm^2/cm^3	
Specific interfacial area of Pt-H_2 electrode	2000 cm^2/cm^3	
H_2 reference concentration	1.461d-3 mol/cm^3	*
O_2 reference concentration	1.529d-3 mol/cm^3	*
Reference concentration	7.1d-3 mol/cm^3	*

Experimental data for charging at various rates and a constant temperature of 10°C were used to validate the present model. Figure 2 compares the experimental cell potential curves with those predicted. The general shape compared well. The quick rise during initial charging was captured, and the second plateau was reproduced. At lower rates there is an under-prediction of the potential and as the rate increases there is a slight overprediction. Because a single set of parameters was kept for all simulations the observed discrepancies were expected.

Figure 3 compares cell pressure variations measured experimentally with the present model predictions. It plots the cell's pressure against time. Excellent agreement is shown for all three charging rates. The change in cell pressure is approximately linear until the overcharge period begins. At that point the pressure rise becomes strongly non-linear.

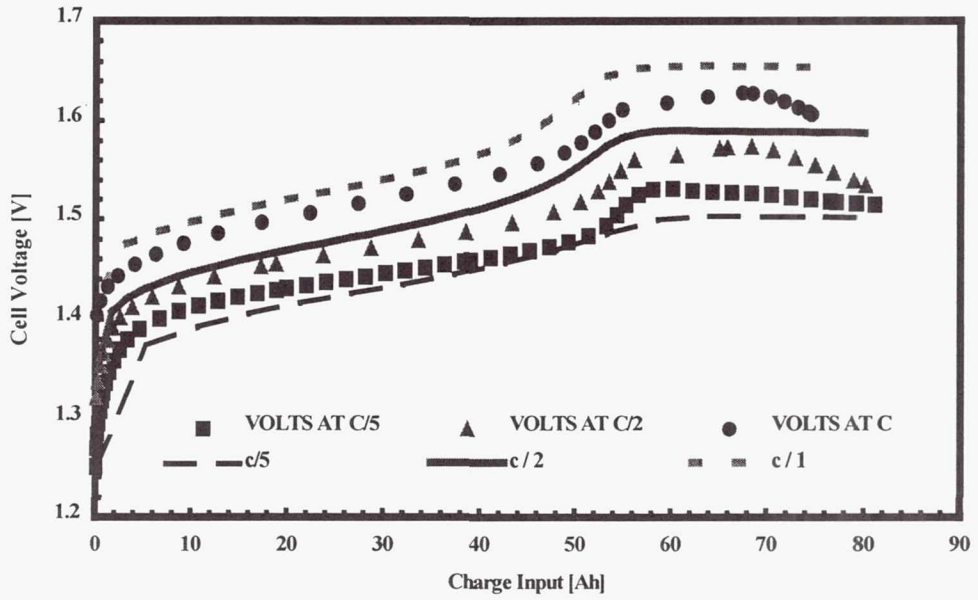

Fig. 2: Comparison of predicted and measured charge curves for a Ni-H_2 cell at different charge rates and constant 10°C. The lines are simulation results, and the symbols denote experimental data.

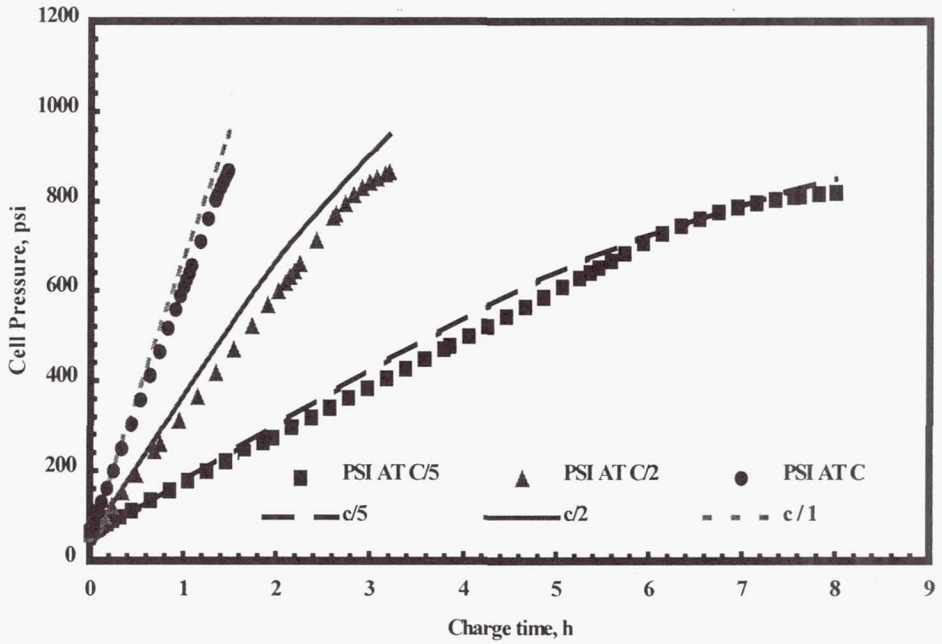

Figure 3. Comparison of experimental and simulated pressure variations for charging at various rates at 10°C.

The following results obtained from the computer simulation are intended to further reveal the internal processes of the Ni-H_2 cell during charge.

Figure 4 plots the reaction current distributions within the nickel electrode when the cell is being charged at a rate of C/1 and a constant temperature of 10°C to 50% charge input. As discussed earlier there are both primary reactions and secondary reactions that occur in the nickel electrode. Theoretically, prior to reaching 100% charge input the primary reactions are the principle reactions. Beyond 100% charge input the secondary reactions take over as the major reactions. Figure 4 clearly shows that for 50% state of charge the primary reactions, 1a and 1b, are dominant. It is also important to note that these reactions are stronger at the electrode/electrolyte interface than at the back of the electrode. Inspection of the chemical reactions, 1a and 1b, reveals that OH^- is a reactant during charging. A large supply of OH^- explains why the reaction is more intense at this location.

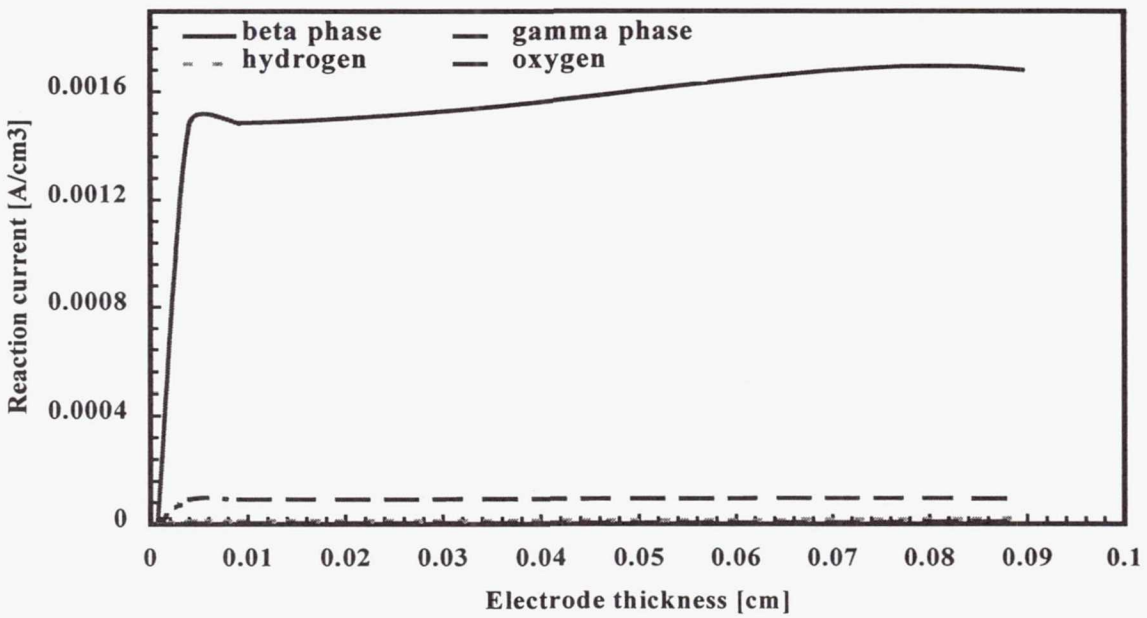

Figure 4: Reaction current distribution inside the nickel electrode for a cell charged at C/1 at constant 10°C to 50 % charge input.

Figure 5 also shows the reaction current distribution within the nickel electrode when the cell is being charged at C/1 and kept at 10°C. It is charged to 150% charge input in this case. As expected, the simulation shows that the primary reactions diminish to approximately zero and the secondary reactions develop once the battery has been charged to 100% charge input. The oxygen and hydrogen reactions, 2 and 3, become the dominant reactions once the 100% point is passed. Also, from Fig. 5 it can be noted that the secondary reaction rates are larger at the electrode/electrolyte for the same reason as stated previously.

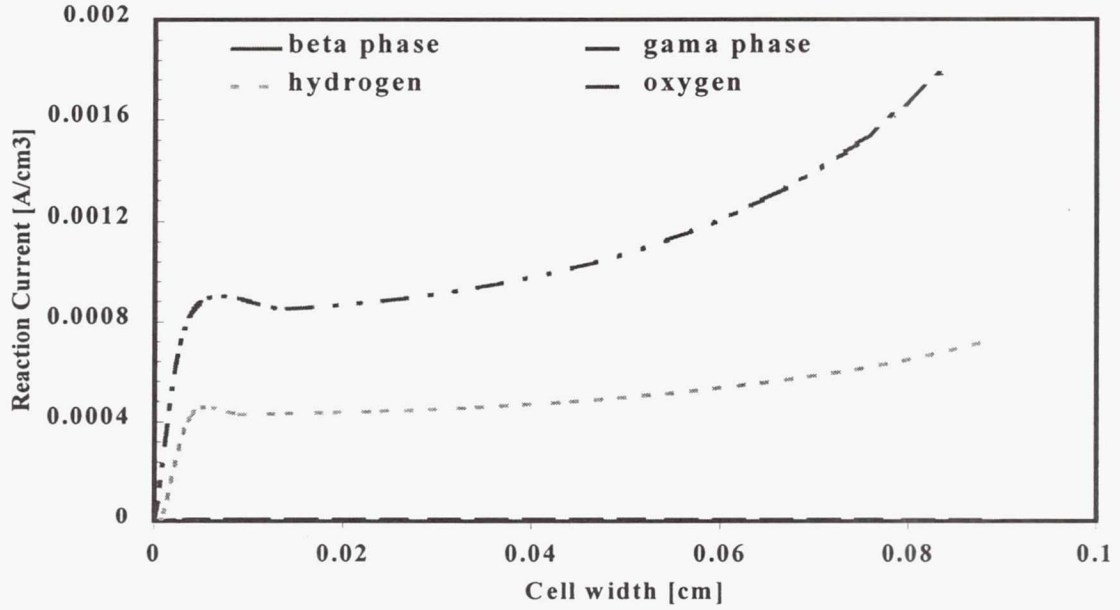

Figure 5: Reaction current distribution within the nickel electrode of a cell charged at C/1 at constant 10°C to 150 % charge input.

Figure 6 plots the reaction currents in the nickel electrode as a function of the charge input relative to the cell capacity. The primary reactions are seen to dominate until 100% charge input is reached, beyond that point the secondary reactions take over. Also to be noted is that the total current prior to and after 100% charge input remains the same.

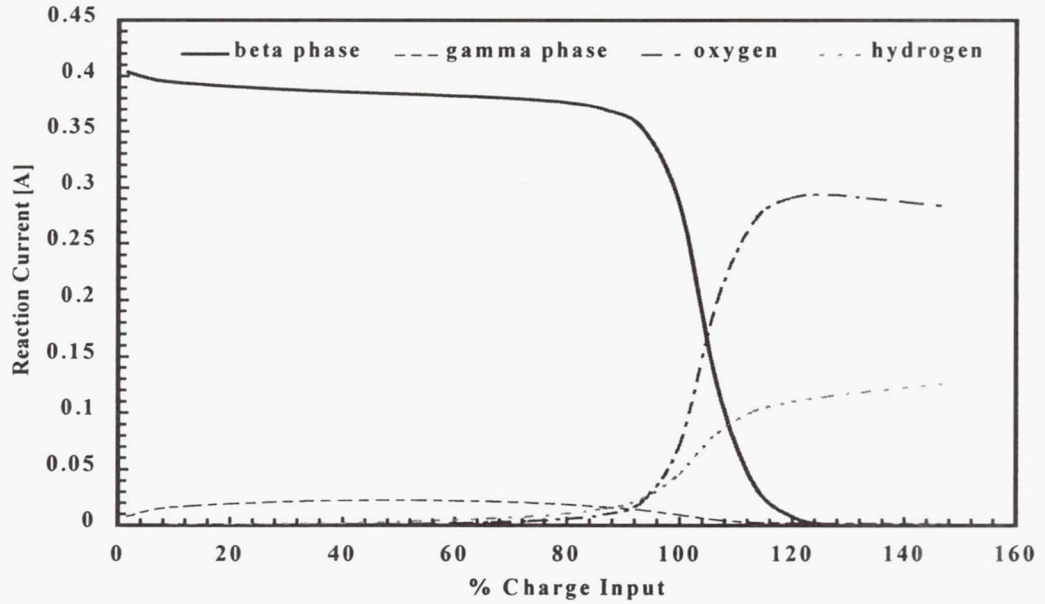

Figure 6. Reaction currents within a cell charged at C/1 and constant 10°C as a function of percent charge input.

Figure 7 plots the partial pressures of the hydrogen and oxygen within a cell charged at C/1 and 10°C. As expected, the increase of pressure due to the hydrogen reaction is dominant. The primary reaction at the hydrogen electrode is the main contributor prior to 100 % charge input, and beyond 100 % the secondary hydrogen reaction at the nickel electrode is adding to the pressure increase. Also at 100 % charge input and beyond the secondary oxygen reaction at the nickel electrode begins, producing a rise in pressure and contributing to the overall increase in pressure.

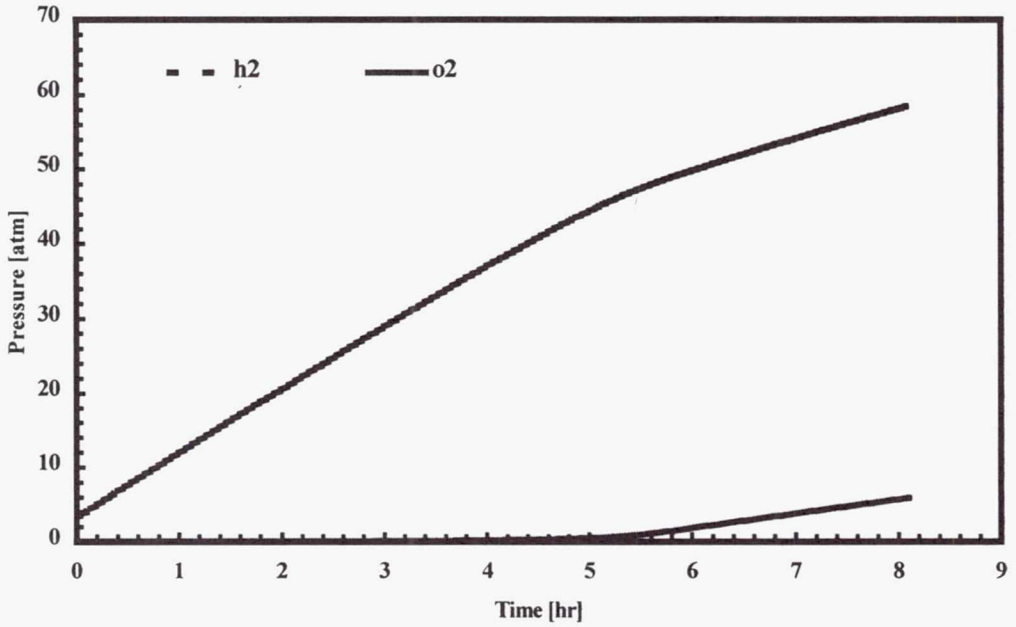

Figure 7: Partial pressures within a cell charged at C/1 and 10°C to 150% of the cell capacity as a function of time.

Figure 8 explores the thermal effects within the cell, showing the temperature profile within the cell with respect to the cell radius. As mentioned earlier the cell is shaped like a disk with a hole at its center. The cell is hottest near the inner edge of the hole and the temperature decreases as the outer diameter of the cell is approached, this is expected based on the boundary conditions. A temperature change of 3°C is seen. A temperature difference of this magnitude influences the kinetic rates of the reactions by as much as 10%.

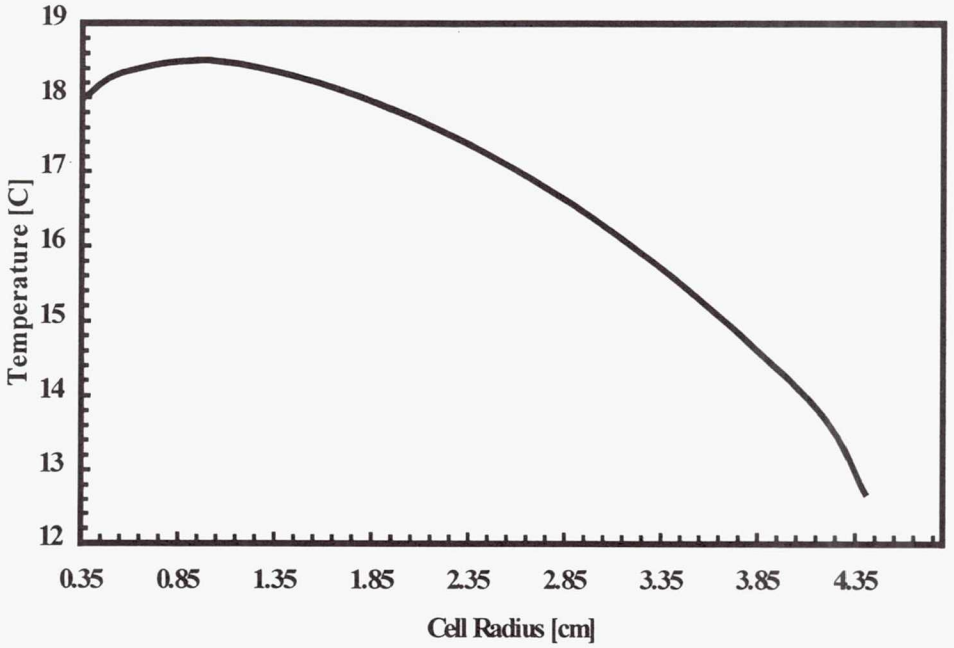

Figure 8: Average temperature of the cell charged at C/1 to 150% of its capacity as a function of the radius with h = 5 W/m^2K.

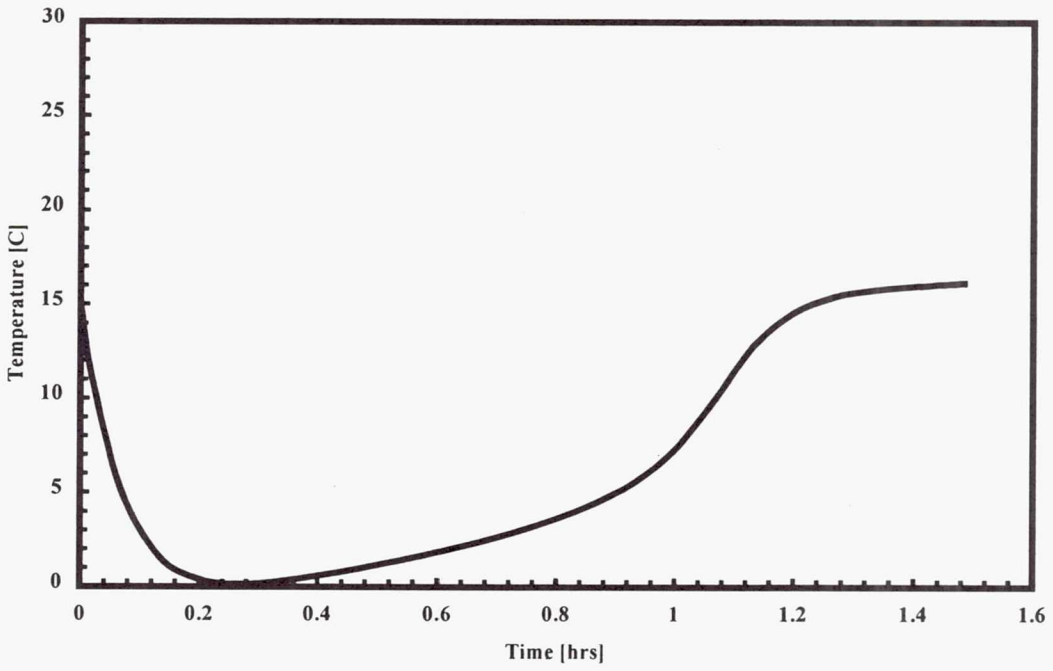

Figure 9: Average temperature of a cell charged at C/1 to 150% of its capacity as a function of time, when h = 5 W/m^2K and $T_{initial}$ = 15°C.

Figure 9 is a graph of the change in average cell temperature with time for a cell charged at C/1. This plot shows an initial temperature drop during the early stages and then an increase in temperature during the later times. At the end of the charging period the battery is hotter than it was initially. The primary reactions dominate when the charging time is less than one hour. It is known that the primary reactions are endothermic [5], therefore explaining the temperature drop during the beginning stages of charging. The hydrogen reaction at the hydrogen electrode is exothermic as is the hydrogen side reaction at the nickel electrode. The hydrogen reactions coupled with resistive heating cause the temperature rise as charging progresses [2].

Experimental temperature measurements were made at the pressure vessel seam. This data was then plotted versus the charging time, as shown in Figure 10. An initial drop in temperature is followed by a strong increase in temperature. Qualitatively Figure 9, the simulation results for the average temperature of the cell, demonstrates a trend very similar to the temperature profile found through external measurements as seen in Figure 10.

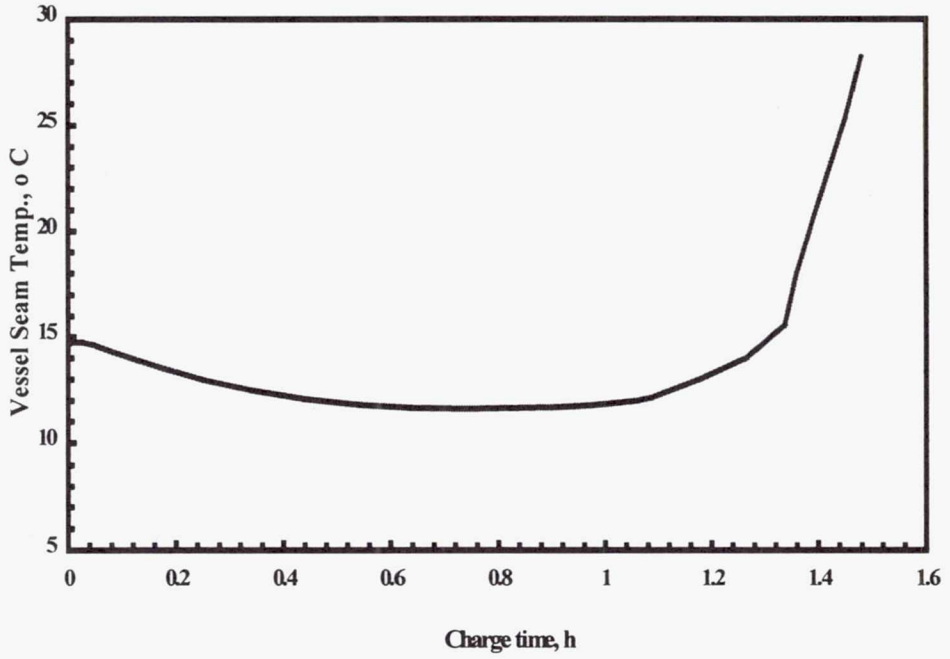

Figure 10: Experimental pressure vessel temperatures plotted as a function of the charging time for a cell charged at C/1.

Figure 11 addresses two important points. It plots the cell proton concentration contour for a cell charged at C/1 to 50 % of the cell capacity. It demonstrates the necessity of having two-dimensionality in the model. The plot shows that the proton concentration varies in both the axial and radial directions. It also shows the effect of temperature on the cell. The proton depletion is greater at the inner diameter of the cell, this is related to the higher temperatures at this location, clearly demonstrating the thermal, electrochemical link. Also, as was noted earlier, there is larger proton concentration depletion along the electrolyte interface due to the plentitude of OH^-.

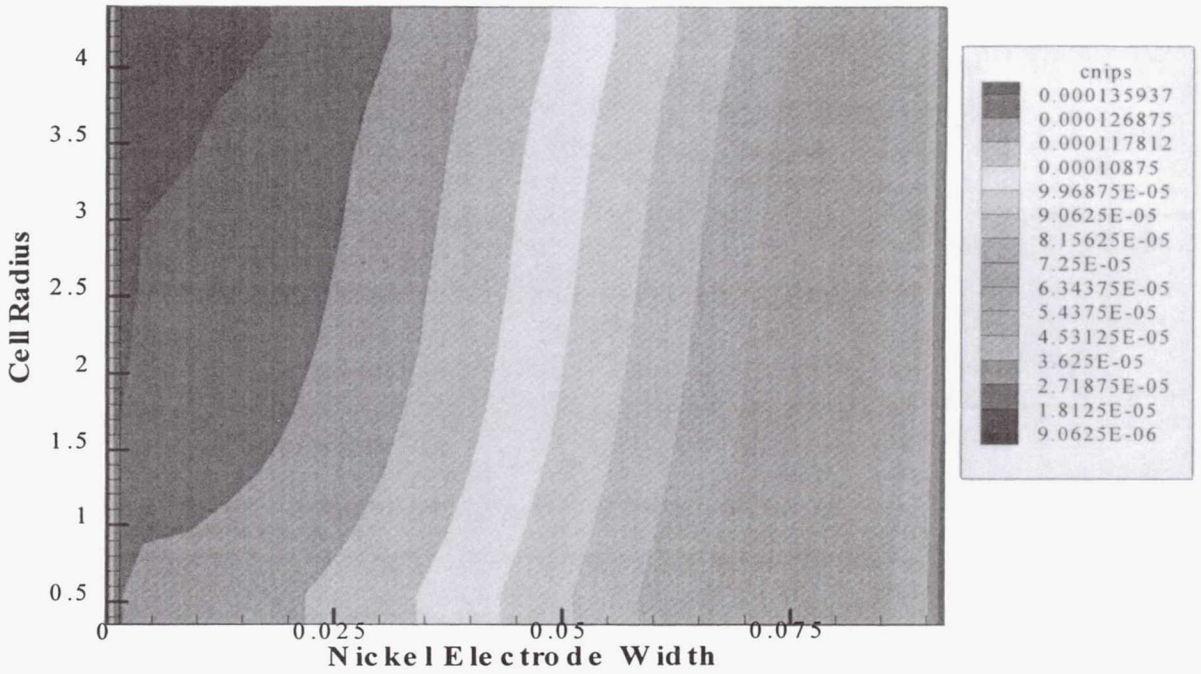

Figure 11: Proton concentration in a cell charged at C/1 to 50 % the cell capacity.

Conclusions:

A two-dimensional, fully coupled, thermal and electrochemical Ni-H_2 model has been developed. Comparison with experimental data validates the model's results. This model complements experimentation by allowing the user to understand occurrences within the cell for various conditions and for many different charging rates. Examples of the program capabilities have been given. Work is underway to expand this model to the entire cell stack, and the thermal interactions between the cells that arise due to this change will be addressed and investigated.

References

1. P. De Vidts, J. Delgado, R. White, *J. Electrochem. Soc.*, **143**, 3223 (1996).
2. P. De Vidts, J. Delgado, B. Wu, D. See, K. Kosanovich, R.E. White *J.Electrochem. Soc.*, **145**, 3874 (1998).
3. J.D. Dunlop, G.M. Rao, and T.Y. Yi, *NASA Handbook for Nickel-Hydrogen Batteries,* NASA reference publication 1314 (1993).
4. W.B. Gu and C.Y. Wang, "Thermal-Electrochemical Modeling of Battery Systems", *J. Electrochem.*, submitted for publication 1999.
5. C. F. Holmes and A.R. Landgrebe, *Batteries for Portable Applications and Electric Vehicles,* The Electrochemical Society Inc., Pennington, NJ (1997).
6. B. Ratnakumar, P. Timmerman, D. Perrone, S. Di Stefano, *Proceedings of 31st Intersociety Energy Conversion Engineering Conference,* **1**, 374 (1996).
7. P. Timmerman, R. Bugga, S. DiStefano, NASA Battery Workshop, 1996.
8. C.Y. Wang, W.B. Gu, and B.Y. Liaw, *J. Electrochem. Soc.*, **145**, 3407 (1998)

List of Symbols

a	specific interfacial area, cm^2/cm^3
c^i	volume-averaging concentration of species i over a phase, mol/cm^3
C_p	specific heat, J/g/K
D^i	diffusion coefficient of species i in a phase, cm^2/s
E_{act}	activation energy, J/mol
F	Faraday's constant, 96,487 C/mol
h	heat transfer coefficient, W/m^2K
i_{nj}	area-averaged transfer current density of reaction j, A/cm^2
$i_{oj,ref}$	exchange current density of reaction j at reference conditions, A/cm^2
j^i	reaction current density due to production or consumption of species i, A/cm^2
k	thermal conductivity, W/mK
q'''	heat generation term
R	universal gas constant, 8.3143 J/mol K
R_{sb}	electrical resistance from solid/substrate interface to the bulk of solid, $\Omega\ cm^2$
t	time, s
t^o_-	transference number of OH^- with respect to the solvent velocity
T	absolute temperature of the cell system, K
$U_{j,ref}$	open-circuit potential for reaction j at reference conditions measured with respect to a Hg/HgO reference electrode, V
V_i	volume of a phase, cm^3

Greek Symbols

α_{aj}, α_{cj}	anodic and cathodic transfer coefficients for reaction j
Δh	enthalpy change
ε_i	volume fraction of a phase in the reference volume fraction
η_j	surface overpotential of electrode reaction, j, V
Φ	general symbol representing a property at a temperature T
λ	thermal conductivity, W/m^2K
Π	Peltier coefficient
ϕ	potential in a phase, V
ρ	density of a species I, g/cm^3
σ	thermal conductivity W/m^2K